Evolution of faint radio sources in the VIDEO-XMM3 field

K.McAlpine[1], M.J.Jarvis[1,2] and D.G.Bonfield[3]

[1] *Department of Physics, University of the Western Cape, Private Bag X17, Bellville, 7537, South Africa*
[2] *Department of Physics, University of Oxford, Denys Wilkinson Building, Keble Road, OX1 3RH, UK*
[3] *School of Physics, Astronomy and Mathematics, University of Hertfordshire, College Lane, Hatfield AL10 9AB, UK*

ABSTRACT

It has been speculated that low luminosity radio-loud AGN have the potential to serve as an important source of AGN feedback, and may be responsible for suppressing star-formation activity in massive elliptical galaxies at late times. As such the cosmic evolution of these sources is vitally important to understanding the significance of such AGN feedback processes and their influence on the global star-formation history of the universe.

In this paper we present a new investigation of the evolution of faint radio sources out to $z{\sim}2.5$. We combine a 1 square degree VLA radio survey, complete to a depth of 100 μJy, with accurate 10 band photometric redshifts from the VIDEO and CFHTLS surveys. The results indicate that the radio population experiences mild positive evolution out to $z{\sim}1.2$ increasing their space density by a factor of $\sim$3, consistent with results of several previous studies. Beyond $z{=}1.2$ there is evidence of a slowing down of this evolution. Star-forming galaxies drive the more rapid evolution at low redshifts, $z{<}1.2$, while more slowly evolving AGN populations dominate at higher redshifts resulting in a decline in the evolution of the radio luminosity function at $z{>}1.2$. The evolution is best fit by pure luminosity evolution with star-forming galaxies evolving as $(1+z)^{2.47\pm0.12}$ and AGN as $(1+z)^{1.18\pm0.21}$.

Key words: radio continuum: galaxies - galaxies: active - galaxies: evolution,

1 INTRODUCTION

The study of the evolution of faint radio sources has taken on new significance in recent years due to the realisation that AGN play an important role in shaping the star formation properties of the galaxies they inhabit (for a review see Cattaneo et al. 2009). As it is now believed that every galaxy harbours a central supermassive black hole this interplay between AGN accretion and star-formation, as well as the cosmic evolution of AGN, have become vitally important to the process of understanding galaxy formation and evolution. Evidence which points to a link between these processes include the tight correlations found between black hole mass and both stellar bulge mass (Kormendy & Richstone 1995; Magorrian et al. 1998; McLure & Dunlop 2002) and velocity dispersion (Gebhardt et al. 2000; Tremaine et al. 2002; Ferrarese & Merritt 2000) in galaxies in the local universe. While on cosmological scales the increase in star-formation density at higher redshifts is accompanied by a corresponding increase in the number density of actively accreting supermassive black holes (Merloni et al. 2007). Furthermore incorporating AGN 'feedback' in semi-analytic models of galaxy formation produces galaxies whose predicted properties are in better agreement with observations (Croton et al. 2006; Bower et al. 2006) particularly at the bright end of the luminosity function. Despite these promising indications many open questions remain about the nature and significance of such postulated AGN 'feedback' processes and how they proceed as a function of cosmic time.

At μJy levels radio surveys become increasing dominated by star-forming galaxies and low luminosity AGN (e.g. Simpson et al. 2006; Seymour et al. 2007; Huynh et al. 2008; Smolčić et al. 2008; Padovani et al. 2009). As radio waves are unaffected by dust extinction future deep radio surveys can overcome many of the selection biases present in optical and X-ray surveys and offer new insights into the co-evolution of these populations out to high redshifts.

Efforts to clarify the nature of the μJy radio population have already revealed that its composition is more complex than previously believed. It has become widely accepted that radio-loud AGN are in fact powered by two fundamentally different modes of accretion (e.g. Evans et al. 2006; Hardcastle, Evans & Croston 2007). The most powerful radio-loud AGN are typically powered by radiatively efficient accretion of cold gas onto a geometrically thin, optically thick accretion disk (e.g. Shakura & Sunyaev 1973; Novikov & Thorne 1973). This type of accretion powers optical and X-ray selected quasars, and produces high excitation emission lines in the host galaxy spectra. Consequently radio sources powered by this mode of accretion

are referred to as High Excitation Radio Galaxies (HERGs). Low-luminosity AGN are more frequently powered by radiatively inefficient (Best & Heckman 2012) accretion of warm gas (Hardcastle et al. 2007) from the intergalactic medium onto a geometrically thick accretion disk. These Low Excitation Radio Galaxies (LERGs) do not exhibit accretion related X-ray emission (Hardcastle, Evans & Croston 2006) or mid-infrared emission from an obscuring nuclear torus (Ogle, Whysong & Antonucci 2006), which is postulated to hide this X-ray emission from view at certain orientations in quasars (Urry & Padovani 1995). Following the terminology of Croton et al. (2006) these two modes of accretion are referred to as 'quasar' and 'radio' mode respectively. While LERGs and HERGs are present at all luminosities, LERGS are more prevalent at low radio luminosities with HERGS becoming the dominant population at luminosities $>10^{26}$ W Hz^{-1} (Hardcastle, Evans & Croston 2009; Herbert et al. 2010, 2011; Best & Heckman 2012; Hardcastle et al. 2013),

Further complications arise from the discovery that in addition to star-forming galaxies and radio-loud AGN, the μJy radio population also contains a significant contribution from sources that traditionally were classified as radio-quiet AGN (Jarvis & Rawlings 2004; Simpson et al. 2006; Wilman et al. 2008; Padovani et al. 2009; Wilman et al. 2010), where the radio emission is much fainter than typical for radio loud AGN, i.e. in the case of quasars. They exhibit a radio to optical light ratio <10 (see e.g. Kellermann et al. 1989) and are powered by a radiatively efficient accretion mode similar to that in HERGs. Currently the contribution from radio-quiet AGN is estimated to be in the region of 25 per cent (Padovani et al. 2009).

Both modes of AGN accretion have a postulated associated mechanism of feedback which result in star-formation quenching in the host galaxy. In the radiatively efficient 'quasar' accretion mode, feedback occurs as a result of quasar driven winds which systematically remove gas from the galaxy, star-formation and accretion activity terminate abruptly as this process depletes their local fuel supply (Silk & Rees 1998; Di Matteo et al. 2005; Cattaneo et al. 2009).

In the radiatively inefficient 'radio' accretion mode the bulk of the energy from the AGN is emitted as kinetic energy in jets, with very little radiative output from a central accretion disk (Merloni & Heinz 2007). These sources accrete at much lower rates and consequently the total energy output from these AGN is lower than in the radiatively efficient case. However, depending on how efficiently the kinetic energy in the jets is converted to heat in the interstellar gas, these AGN may still have considerable potential to influence the star-formation properties of the galaxies they inhabit as well as their larger scale environments (e.g. McNamara et al. 2000; Bîrzan et al. 2004). Using a scaling relationship between radio luminosity and mechanical heating power derived from cluster observations, Best et al. (2006) demonstrated that the time-averaged energetic output of 'radio' mode accretors was indeed sufficient to counter cooling losses in massive, red galaxies. In this mode the AGN is fuelled by direct accretion of the hot interstellar gas and is also the source of gas heating. As such AGN feedback in this mode has the potential to set up a stable feedback loop where the accretion rate is automatically adjusted by the available supply of hot gas (Allen et al. 2006; Best et al. 2006; Hardcastle et al. 2007).

A key piece of evidence in determining the relative significance of both types of AGN feedback is an accurate determination of the cosmic evolution of the radio sources whose jets are speculated to be enormously influential via this 'radio' mode accretion. It is already well established that powerful radio AGN undergo very rapid evolution with their number densities increasing by a factor of ∼1000 out to redshifts of ∼2 (Longair 1966; Laing, Riley & Longair 1983; Dunlop & Peacock 1990; Willott et al. 2001), with evidence of a decline in their number density taking place beyond z∼3 (Jarvis & Rawlings 2000; Jarvis et al. 2001; Wall et al. 2005; Rigby et al. 2011). While current studies of the lower luminosity, predominantly LERG, radio population indicate that they experience much milder positive evolution, with density enhancements of the order 2–10 out to z∼1.2 (Clewley & Jarvis 2004; Sadler et al. 2007; Donoso, Best & Kauffmann 2009; Smolčić et al. 2009a; Strazzullo et al. 2010; Padovani et al. 2011; McAlpine & Jarvis 2011). Recent work by Best & Heckman (2012) suggests that the observed mild evolution at low radio luminosities may be primarily driven by the evolution of a small number low-luminosity HERGs. They find that LERG populations experience little or no evolution out to z∼0.3 while HERGs are strongly evolving at all luminosities, but only contribute a small fraction of the low luminosity radio population.

A further division in evolutionary behaviour has been observed between radio-quiet and radio-loud AGN. Studies by Padovani et al. (2009) and Simpson et al. (2012) find very little evidence of evolution in the low-luminosity radio-loud sources and evidence for stronger evolution in the radio-quiet AGN. This possibly provides further evidence of a link between the radio-quiet AGN and the HERG sources which are believed to be powered by the same radiatively efficient accretion mode, and may suggest that it is these 'quasar' mode accretors which undergo the strongest evolution.

This paper presents a new investigation of the evolution of low luminosity radio sources out to z∼2.5. Details of the radio observations and multiband photometry used in this study are presented in sections 2 and 3. The cross matching procedure is outlined in section 4. A description of the photometric redshifts used to construct the radio luminosity function is presented in sections 5. While section 6 presents our results and our conclusion and discussion is presented in section 7. We use AB magnitudes throughout this paper and assume a cosmology of H_0=70 km s^{-1} Mpc^{-3}, Ω_m=0.3, and Ω_Λ=0.7.

2   RADIO DATA

This work utilises the radio survey completed by Bondi et al. (2003) using the Very Large Array (VLA). These observations cover 1 square degree centred at α(J2000)=2^{h}26^{m}00^s and δ(J2000)=−4^{d}30′00″ with 9 pointings. They were taken in the VLA B-configuration and have a FWHM synthesised beamwidth of approximately 6 arcsec while the final mosaiced image has a background rms noise level of ∼17μJy.

A catalogue of 1054 radio sources whose peak fluxes exceed 60μJy was extracted from the mosaiced image us-

ing the AIPS Search and Destroy (SAD) task. To minimize the contribution of spurious sources to the final catalogue sources were retained as real detections only if their peak flux to local noise ratios is >5. Multiple component radio sources are identified in the image by assuming their components meet the following three criteria, they are separated by <18 arcsec, have peak flux ratios <3, and all components have a peak flux >0.4 mJy/beam, only 19 multiple component sources are identified in the field. Further details of the calibration, catalogue extraction and multi-component classification procedures are outlined in Bondi et al. (2003).

Further observations of this field were performed by Bondi et al. (2007) using the GMRT at 610 MHz. The GMRT observations covered the whole square degree of interest with 5 pointings observed for ~5.5 hours each, resulting in a 5σ limiting flux density of $\sim200\mu$Jy. These GMRT observations were used to obtain spectral index estimates of the VLA radio sources after matching within a 3" tolerance. Throughout this paper, wherever a spectral index estimate is required, e.g. in the case of determining radio luminosities, we use the estimates from Bondi et al. (2007). For the 269 sources not detected by the GMRT at 610 MHz we assume a standard spectral index of $\alpha = -0.7$.

3   MULTI-BAND PHOTOMETRY

The square degree of VLA radio observations has been observed with the VISTA Deep Extragalactic Observations (VIDEO; Jarvis et al. 2013) survey. The VIDEO survey is a 12 sq. degree survey over three fields with the Visible and Infrared Survey Telescope for Astronomy (VISTA) whose objective is to study the formation and evolution of galaxies and galaxy clusters from the present day to $z\sim4$. The survey provides photometry in the Z,Y,J,H and K_s bands to 5σ depths (2 arcsec apertures) of 25.7, 24.6, 24.5, 24.0, 23.5 magnitudes respectively. This field also coincides with the Canada-France-Hawaii Telescope Legacy Survey D1 field (CFHTLS D1; Ilbert et al. 2006) which provides additional photometry in the u*,g',r',i',z' optical bands to depths of 26.5, 26.4, 26.1, 25.9, 25.0.

4   CROSS-MATCHING

Single component radio sources were matched to their infrared counterparts using the Likelihood Ratio (LR) technique (de Ruiter et al. 1977; Sutherland & Saunders 1992; Ciliegi et al. 2003). The LR is a commonly used method to associate low resolution radio observations with higher resolution optical or infrared observations. In brief, it calculates the ratio of the probability that a given source and counterpart are related to the probability that they are unrelated. This probability takes into account the positional accuracy of the near infrared and radio observations as well as the magnitude distributions of the background infrared sources and the radio source counterparts. Full details of the cross-matching procedure between the VIDEO survey and the Bondi et al. (2003) VLA observations are discussed in McAlpine et al. (2012).

The procedure resulted in a cross-matched catalogue of 942 radio sources whose counterparts are brighter than

$K_s \sim23.8$. This represents a completeness of 91.0 per cent, the percentage of misidentified counterparts in this catalogue is predicted to be very low at the level of ~0.8 per cent.

Multiple component radio sources were associated with their counterparts via visual inspection. These sources are less suited to the LR method used for single component sources as the likely position of the counterpart source and the associated errors on this position are poorly constrained. There are 19 multiple sources in this field and only 9 of these were associated with an infrared counterpart.
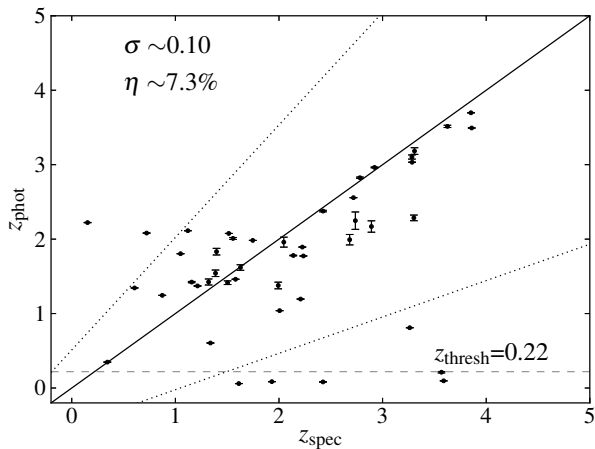
5   PHOTOMETRIC REDSHIFTS

Photometric redshifts for the combined VIDEO and CFHTLS datasets have been determined using the publicly available code Le Phare[1] (Ilbert et al. 2006). This code derives photometric redshifts via a Spectral Energy Distribution (SED) fitting method. It operates by shifting a set of input template SEDs, assumed to be representative of the true SED profiles of the observed sources, to a range of redshifts and fitting these to the observed photometry. The redshift of the best fitting template is then adopted as the best photometric redshift estimate.

The accuracy of the photometric redshifts was assessed by comparing with spectroscopic redshifts in the VIMOS VLT deep survey (VVDS; Le Fèvre et al. 2005), which is a deep spectroscopic survey limited to $I_{AB} \sim24.0$. Comparing to sources with very secure spectroscopic redshifts and excluding sources identified as quasars, the sample has a normalised median absolute deviation (NMAD) in $\frac{\Delta z}{(1+z_s)}$ of $\sigma \sim0.025$, where $\Delta z = |z_p - z_s|$ (see Ilbert et al. 2006). Approximately 3.8 per cent of the sources are catastrophic outliers, defined as cases where $\frac{\Delta z}{(1+z_s)} > 0.15$. Further details of the procedure used to derive these photometric redshifts are provided in the VIDEO survey description paper (Jarvis et al. 2013).

5.1   Quasar photometric redshifts

As some fraction of the radio sources will be associated with quasars we conducted an investigation into the photometric redshifts of quasars in the VIDEO survey. Photometric redshifts determined for quasars are generally much less reliable than those obtained for galaxies due to the absence of strong spectral break features which provide the strongest constraints in the SED fitting procedure (see e.g. Richards et al. 2001; Babbedge et al. 2004; Mobasher et al. 2004; Polletta et al. 2007). Quasar SEDs are generally well represented by a power law continuum overlaid with a series of broad and narrow emission line features. As a power law spectrum is invariant under redshift, constraints in the photometric redshift fitting procedure rely on the quasar emission line features. Success thus depends on the emission line features having sufficient flux to influence the measured broad-band photometry. These emission lines are clearly difficult to identify and accurately localise based solely on the

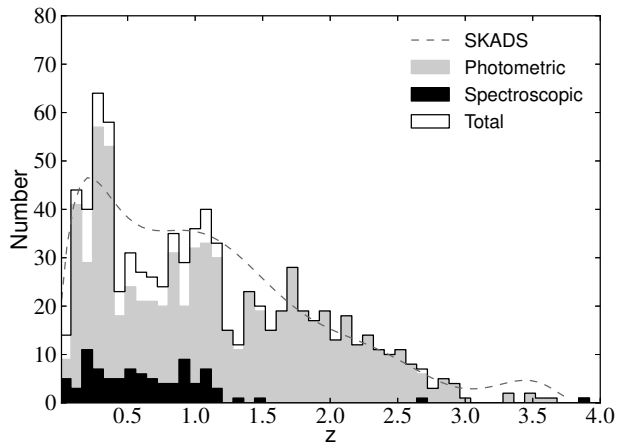[1] http://www.cfht.hawaii.edu/ arnouts/LEPHARE/lephare.html

Figure 1. Photometric versus spectroscopic redshifts for objects identified as quasars in the VVDS. The sample has a NMAD in $\frac{\Delta z}{(1+z_s)}$ of $\sigma=0.10$ and approximately 7.3 per cent of the objects are 5σ outliers. Photometric redshifts below the z_{thresh} level, plotted as a dashed line, are clearly not reliable. Dotted lines are plotted at 1σ. The error bars represent the 1σ errors derived from distribution of χ^2 values as a function of z as described in section 5.3.

final integrated flux measurements, and may also fall between gaps in the filter coverage. Further sources of error include the possibility of strong contamination of the AGN SED by the host galaxy as well as the intrinsic variability of quasars. As most surveys have non-simultaneous photometry this variability hampers the construction of a typical snapshot SED for fitting. These factors culminate in the effect that the most accurate photometric redshifts for quasars, using a variety of techniques to mitigate these limitations, produce photometric redshifts with dispersions in $\frac{\Delta z}{(1+z_s)}$ of ~0.35 (see Ball et al. 2008; Salvato et al. 2009, 2011) whilst for galaxies much simpler techniques routinely report estimates $\frac{\Delta z}{(1+z_s)}$ ~0.1 or even much lower values (Wolf et al. 2004; Ilbert et al. 2006, 2009; Cardamone et al. 2010; Jarvis et al. 2013).

To determine the severity of this reduced accuracy in photometric redshift estimates, in figure 1 we show photometric versus spectroscopic redshifts for the 73 sources identified as quasars in the VVDS survey. These were classified as quasars due to the presence of broad emission line features in their spectra. Only sources with secure redshifts were retained for comparison. There is a clearly discernable threshold in figure 1, at $z_{\text{phot}}=0.22$, below which the photometric redshifts are unreliable. Reassuringly the photometric redshifts of the remaining objects appear to be well correlated with spectroscopic redshift, although there is a larger spread in $\frac{\Delta z}{(1+z_s)}$ than for the general galaxy population. This quasar sample has a NMAD in $\frac{\Delta z}{(1+z_s)}$ of $\sigma\sim0.10$ and ~7.3 per cent of the sample are catastrophic outliers with $\frac{\Delta z}{(1+z_s)}>5\sigma$.

As figure 1 indicates that quasars with $z_{\text{phot}}<0.22$ may be unreliable, we attempted to identify such potentially problematic sources in our sample. Candidate quasars were identified based on their SEXTRACTOR (Bertin & Arnouts 1996) CLASS_STAR parameter which provides a measure of how well resolved an object is in the infrared images. A criteria of CLASS_STAR>0.8 identified 78 potential quasars

Figure 2. Redshift distribution of all radio sources with counterparts in the VIDEO survey. Objects with spectroscopic redshifts in the VVDS are plotted in black, while photometric redshifts are indicated in grey. The redshift distribution predicted by the SKA simulated skies (SKADS, Wilman et al. 2008, 2010) is overplotted by the dashed line.
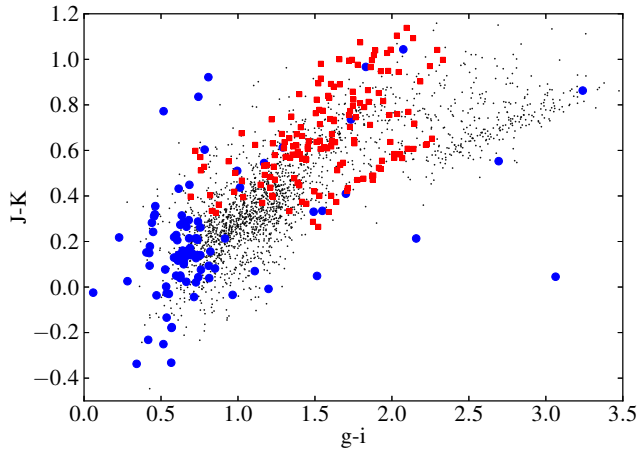
in the VLA survey and eight of these have photometric redshifts of <0.22. To determine the effect of these potentially poor redshift estimates on our conclusions we calculate the RLF in section 6 both including and excluding these 8 sources and find the results of our analysis to be unchanged.

5.2   Redshift Distribution

The redshift distribution of all radio sources with counterparts in the VIDEO survey is presented in figure 2. Objects with spectroscopic redshifts in the VVDS survey are plotted in black. A notable feature of this plot is a large peak in the distribution at redshifts of $z\sim0.2$–0.4.

The origin of this peak is unclear as there are no corresponding large peaks in the redshift distribution of the full VIDEO infrared catalogue. Objects with poor photometric redshift estimates in the VIDEO survey were found to be preferentially associated with bluer colours (Jarvis et al. 2013). To determine whether the large peak at $z\sim0.2$–0.4 could be caused by a failure in the photometric redshift estimation process we compare the colour distribution of radio sources with $0.2<z_{\text{phot}}<0.4$ to the colour distribution of NIR sources whose $\frac{\Delta z}{1+z_{\text{spec}}}>0.15$. It is clear from figure 3 that the low redshift radio sources do not occupy the bluer region of the g-i, J-K colour diagram associated with poor redshift estimates, tending to suggest that these estimates are reasonably reliable and the observed peak is a real feature of the radio sources in this field. There is also a small peak visible in the spectroscopic redshifts in figure 2 at $z\sim0.2$–0.4 that adds weight to our assertion that the photometric redshifts are reliable.

The feature at $z\sim0.2$–0.4 could plausibly be due to large-scale structure within this relatively small field. We note that there are six known X-ray clusters at z=0.262, 0.266, 0.293, 0.301, 0.307 and 0.345 (Pacaud et al. 2007; Adami et al. 2011) in this field which are at least partially responsible for an increase in the galaxy density within this redshift range. However, we also note that we expect there to
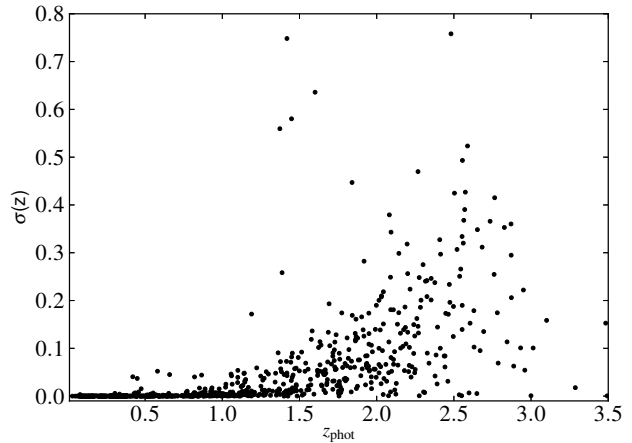
Figure 3. *g-i* versus *J-K* colour diagram. Photometric redshift outliers with $\frac{\Delta z}{1+z_{\rm spec}}$ >0.15 are indicated by blue dots, while radio sources with $0.2<z_{\rm phot}<0.4$ are plotted as red squares. The outlier sources preferentially occupy the bottom left hand corner of the diagram and show little overlap with the low redshift radio sources in their colour distribution.

be an overdensity of radio sources around this redshift range due to the fact that star-forming galaxies can be detected to $z\sim0.4$ in our radio data, whereas beyond this redshift the radio source population becomes dominated by AGN, as is apparent from the SKADS simulations shown in figure 2.

5.3   Photometric Redshift Errors

Comparison with spectroscopic redshifts provides an important characterization of the variance and fraction of failures in the photometric redshift estimates, however this process cannot be used to identify the photometric redshifts in the full sample which are most likely to be unreliable. Extra information regarding the reliability of individual redshift estimates can be extracted by considering whether the fitting procedure used to produce it was well constrained by the available photometry or not. A measure of the uncertainty in the photometric redshift estimate can thus be obtained directly from the χ^2 distribution obtained when fitting the template to the observed photometry. A redshift probability density function (PDFz) is constructed from the χ^2 values as PDF$z \propto \exp\left(-\frac{\chi^2}{2}\right)$. The 1$\sigma$ confidence intervals are predicted by determining the redshifts corresponding to an increment in the χ^2 value of $\Delta\chi^2=1$, while 3σ errors are determined at $\Delta\chi^2=9$.

Errors produced by this method do not account for intrinsic uncertainties in the photometry not included in the measured photometric errors such as those caused by blending or the presence of bright neighbours, nor can they account for inadequacies in the input template library. They are nevertheless useful indicators of reliability in the absence of spectroscopic data and Ilbert et al. (2006) demonstrated that 68 per cent and 92 per cent of the spectroscopic redshifts are located within the 1σ and 3σ errors respectively. Figure 4 presents the errors estimated from the χ^2 fitting for the radio sources in this sample. This figure demonstrates that the uncertainty in the fitting procedure, and consequently the redshift estimates, increases significantly

Figure 4. The 1σ errors on photometric redshift estimates as a function of redshift.

towards higher redshifts. This is to be expected due to the larger errors on faint photometry towards high redshift objects as well as the possibility that the locally observed, empirical templates used in the SED fitting procedure are not sufficiently representative of these high redshift objects. These larger errors towards higher redshifts are accounted for in our determination of the Radio Luminosity Function (RLF) via Monte Carlo simulations which account for the probability distribution in $z_{\rm phot}$ for each radio source.
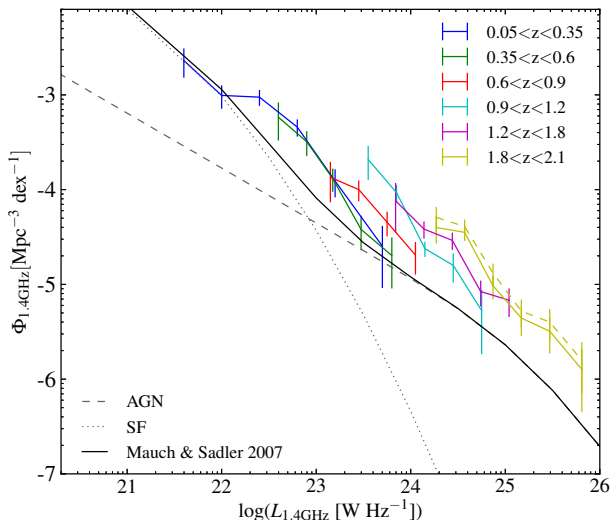
6   RADIO LUMINOSITY FUNCTION

We determine the RLF for the full population of radio sources in six redshift bins using the standard $\frac{1}{V_{\rm max}}$ method (Schmidt 1968). Inclusion in the final cross-matched sample depends on the source exceeding the flux limits of both the radio and near-infrared surveys, thus the final maximum observable redshift $z_{\rm max}$ is calculated as $\min(z_{\rm radio}, z_{\rm IR})$ where $z_{\rm radio}$ and $z_{\rm IR}$ represent the maximum observable redshifts of the source in the radio and infrared surveys respectively. We estimate the maximum $z_{\rm IR}$ by redshifting the best fitting SED template from the photometric redshift estimation procedure and determine the redshift where the template becomes fainter than our imposed magnitude limit of K$_s$=23.8. Similarly for the radio sources we estimate their intrinsic luminosity assuming the standard spectral index based k-correction and determine the redshift at which they drop below the VLA survey flux limit.

Figure 5 presents the RLF in six redshift bins in the interval z=0–2.5, the error bars in the plot incorporate both the errors due to the sample size per bin as well as the uncertainties in the photometric redshift estimates. The latter were estimated using Monte Carlo simulations by constructing 1000 possible realisations of the PDFz of the photometric redshifts, calculating the RLF for each of the realisations and determining the median and standard deviation of these simulated RLFs. Including the effects of uncertainty in the photometric redshifts is particularly relevant in the high redshift bins as figure 4 indicates that these errors increase substantially at z>1.4. In order to account for sample variance in a field of 1 square degree we determine the variance in the

Table 1. The variance on the number of radio sources above 100 μJy in a 1 square degree field as function of redshift, determined from the SKADS simulations (Wilman et al. 2008, 2010)

z	σ [per cent]
0.1–0.35	15
0.35–0.6	13
0.6–0.9	15
0.9–1.2	18
1.2–1.8	14
1.8–2.5	14

Figure 5. Radio luminosity function in six redshift bins to $z{\sim}2.5$. The error bars incorporate the uncertainty in photometric redshifts, estimated via Monte Carlo simulations. The dashed yellow line represents the change in the RLF which occurs at the highest redshifts assuming that the unmatched radio sources in the VIDEO survey have a redshift distribution similar to the faintest sources, $K_s{>}23.5$, in the SXDF (Simpson et al. 2012) field. The solid black line represents the local luminosity function of Mauch & Sadler (2007) with the contribution of star-forming galaxies and AGN represented by the dotted and dashed lines respectively.

number of sources >100 μJy in 100 1 square degree fields in the SKADS simulations (Wilman et al. 2008, 2010;see also Heywood, Jarvis & Condon 2013). This variance was determined for each of the redshift bins considered in figure 5, and added in quadrature to the errors due to photometric redshift uncertainties. The calculated variances are reported in table 1.

The RLF in this work is compared to the local RLF determined by Mauch & Sadler (2007) using NVSS radio sources with spectroscopic redshifts from the 6 degree Field Galaxy Redshift Survey (6dFGRS; Jones et al. 2004). The Mauch & Sadler (2007) luminosity function is constructed from separate fits to the luminosity functions of star-forming galaxies and AGN, and the individual contributions of these two populations are plotted as dotted and dashed lines in figure 5 respectively. It is clear that the local radio luminosity function is dominated by star-forming galaxies and AGN contributions at low and high luminosities respectively, with the division falling at roughly $\sim 10^{23}$ W Hz^{-1}. There

is a large discrepancy between the VLA-VIDEO local RLF determined in this work and that of the Mauch & Sadler (2007) star-forming galaxy luminosity function at low luminosities (reduced $\chi^2{=}5.9$). This discrepancy is probably caused by the large concentration of objects in the VLA-VIDEO survey in the range $z{\sim}0.2$–0.4 (see figure 2), which can easily be explained by sample variance at these low redshifts, where our volume is relatively small. The absence of higher luminosity radio sources in the lowest redshift bin, due to the small sky area, precludes us from making a direct comparison with the local AGN luminosity function.

6.1 Evolution of combined star-forming and AGN population

Figure 5 appears consistent with a fairly rapid increase in the space density of radio galaxies up to redshifts of $z \sim 1.2$, with hints of a possible slowing down of this process between redshifts $z = 1.2$–2.5. To quantify these broad evolutionary trends we initially use models of both pure density and pure luminosity evolution of the combined star-forming and AGN RLF, such that:

$$\Phi_{\text{PDE}}(z) = (1+z)^{\alpha_d}(\Phi_{\text{SF}} + \Phi_{\text{AGN}}) \quad (1)$$

$$\Phi_{\text{PLE}}(z) = \Phi_{\text{SF}}\left(\frac{L}{(1+z)^{\alpha_l}}\right) + \Phi_{\text{AGN}}\left(\frac{L}{(1+z)^{\alpha_l}}\right) \quad (2)$$

where Φ_{SF} and Φ_{AGN} are the star-forming and AGN luminosity functions of Mauch & Sadler (2007) respectively. $\Phi_{\text{PDE}}(z)$ and $\Phi_{\text{PLE}}(z)$ are the evolved luminosity functions at redshift z assuming pure density and pure luminosity evolution respectively. Such models are clearly limited in their ability to accurately represent the behaviour of the three sub-classes of potentially independently evolving radio sources present in the sub-mJy VLA-VIDEO sample. The parametrization simply provides a convenient means to quantify the overall strength and sense of the evolution taking place at different cosmic times.

Based on the tentative evidence in figure 5 that the evolutionary behaviour of these sources changes at a redshift of $\sim$1.2, we fitted six possible evolutionary scenarios to the data, the first is a pure density evolution model with a single α_d parameter for the entire redshift range from $z{\sim}0$–2.5. The second is of pure density evolution out to a redshift of $z{=}1.0$ and no further evolution taking place beyond this, and the third fits independent pure density evolution parameters α_{d1} and α_{d2} in the redshift $z{\sim}0$–1.2 and 1.2–2.5 ranges. We repeat the fitting procedure for these three scenarios assuming pure luminosity evolution. To avoid the fit being biased by the large discrepancy between the VLA-VIDEO RLF and the Mauch & Sadler (2007) RLF at low redshifts we excluded the $z{<}0.35$ points from the fit.

The evolution parameters and χ^2 values determined from these fits are presented in table 2, and figure 6 presents a comparison of the data points to the evolved luminosity function produced by the best fitting model. In all cases the data implies an increasing source density out to $z{\sim}1$, with density enhancements at this redshift of a factor of $\sim$3 over the local values. The independent α_{d2} and α_{l2} determined in model 3 imply an increase in space density towards earlier cosmic times but are also consistent with the scenario of no evolution beyond $z{\sim}1.2$ (within 2σ). A constant positive

Table 2. Results of fitting three different evolutionary scenarios to the RLF in six redshift bins. Pure density evolution is assumed in all three cases.

| | | z=0–1.2 | z=1.2–2.5 | | |
		α_{d1}	α_{d2}	χ^2	reduced χ^2
PDE	model 1	1.28±0.88		34.61	1.44
PDE	model 2	1.53±0.11	0±0	36.48	1.52
PDE	model 3	1.38±0.17	0.23±0.16	33.63	1.46

Table 3. Results of fitting three different evolutionary scenarios to the RLF in six redshift bins. Pure luminosity evolution is assumed in all three cases.

| | | z=0–1.2 | z=1.2–2.5 | | |
		α_{l1}	α_{l2}	χ^2	reduced χ^2
PLE	model 1	1.72±0.11		34.67	1.45
PLE	model 2	2.03±0.13	0±0	33.03	1.37
PLE	model 3	1.90±0.17	0.26±0.19	30.66	1.33

evolution across the entire redshift range provides a better fit to the data in the pure density evolution case, while a slower evolution beyond $z{\sim}1.2$ is a better fit for pure luminosity evolution.

Recent results from Simpson et al. (2012) identified tentative evidence of a decline in the RLF of radio sources at redshifts >1.5 in the luminosity range $10^{24-25.5}$ W Hz^{-1} (see their figure 11), however the VLA-VIDEO RLF consistently increases with redshifts even beyond $z{\sim}1$. Rigby et al. (2011) also identify a luminosity dependent turnover in the luminosity function, with lower luminosity objects experiencing a decline in their number densities at lower redshifts than their high luminosity counterparts. Their results imply a turnover at $z>0.7$ for objects with luminosities in the 10^{25-26} W Hz^{-1} range, which is at a slightly lower redshift than seen in the VIDEO-VLA RLF. The points in figure 5 do not betray any hint of such a luminosity dependent effect. However the use of a single flux-density limited sample restricts our investigation to a narrow luminosity range in each redshift bin hampering any attempt to confirm this.

6.2 Evolution of separate star-forming and AGN populations

AGN and star-forming populations may evolve independently from one another and there is some evidence that low luminosity AGN evolve more slowly than star-forming galaxies up to $z{\sim}1.2$ (e.g. Smolčić et al. 2009a,b). Figure 5 indicates that at low redshifts we are primarily probing luminosities dominated by star-forming galaxies, whereas at higher redshifts the the radio source population is dominated by contributions from AGN. Thus the observed decline in the evolution of the LF towards higher redshifts ($z>1.2$) could be explained if the AGN population evolved more slowly than the star-forming galaxies in the $z<1.2$ interval. To further investigate the separate contributions of star-forming galaxies and AGN to the evolution of the total RLF we fit a two component model of pure density and pure luminosity evolution. This model allowed the star-forming and AGN populations to evolve independently such that:

$$\Phi_{\mathrm{PDE}}(z) = (1+z)^{\alpha_d^{\mathrm{AGN}}}\Phi_{\mathrm{AGN}} + (1+z)^{\alpha_d^{\mathrm{SF}}}\Phi_{\mathrm{SF}} \qquad (3)$$

Table 4. Results of fitting independently evolving star-forming and AGN luminosity functions to the RLF, both pure density evolution (PDE) and pure luminosity evolution (PLE) are considered.

| | SF | AGN | | |
	α^{SF}	α^{AGN}	χ^2	reduced χ^2
PDE	3.50±0.40	1.16±0.09	24.52	1.06
PLE	2.47±0.12	1.18±0.21	20.64	0.89

$$\Phi_{\mathrm{PLE}}(z) = \Phi_{\mathrm{SF}}\left(\frac{L}{(1+z)^{\alpha_l^{\mathrm{SF}}}}\right) + \Phi_{\mathrm{AGN}}\left(\frac{L}{(1+z)^{\alpha_l^{\mathrm{AGN}}}}\right) \; (4)$$
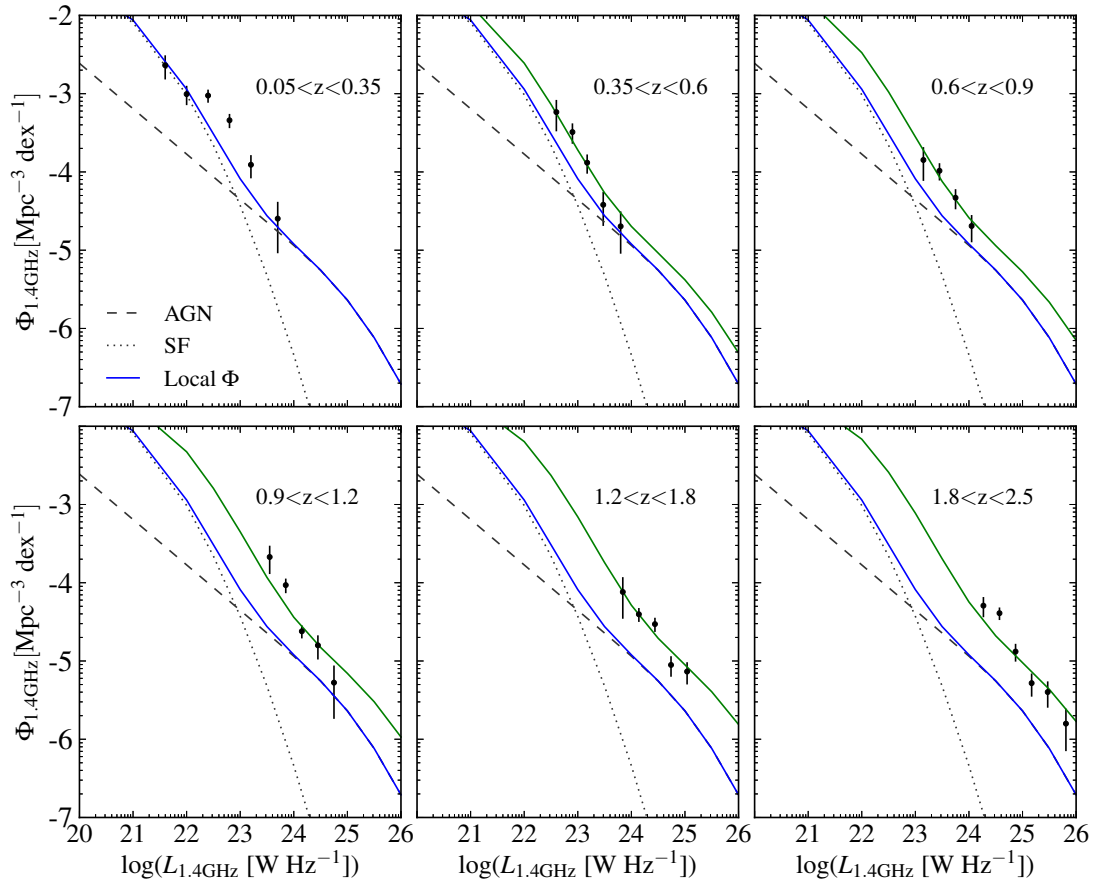
Fitting separate α_l and α_d values for AGN and star-forming galaxies resulted in much lower reduced χ^2 values than the single component model in section 6.1. The AGN population was found to evolve more slowly than the star-forming population, thus confirming that the AGN are responsible for the slower evolution beyond $z{\sim}1.2$ detected in the single component fit. The results of the fit are presented in table 6.2 and figure 7 compares the best fit two component model with the measured RLF.

6.2.1 Template Classification

The template fitting used in section 5 to derive photometric redshifts can be used to distinguish galaxies which are star-forming from those with predominantly old stellar populations. As the low luminosity radio AGN population is dominated by LERGs (Best & Heckman 2012) which are preferentially hosted in red passively evolving galaxies (Baldi & Capetti 2008; Herbert et al. 2010; Smolčić & Riechers 2011; Best & Heckman 2012) a template based classification scheme can be used to roughly separate the radio population into its AGN and star-forming components. The photometric redshift fitting procedure is based on templates interpolated from six observed spectra an elliptical, two spirals and and irregular galaxy as well as two observed starburst templates. We identified AGN in the radio population as sources redder than the spiral galaxy templates. The resulting AGN and star-forming RLF's, shown in figures 8 and 9, were found to be consistent with the fit presented in figure 7 for these two populations out to $z{\sim}1.2$. At higher redshifts this agreement breaks down and a large fraction of the AGN at $z>1.2$ are associated with bluer star-forming templates.

There are several possible reasons for this, fainter photometry and greater uncertainty in the level of dust-extinction towards high redshift objects make it harder to accurately constrain their intrinsic underlying SEDs, thus the colour classification at these redshifts may no longer be reliable. A second possibility is raised by the results of Janssen et al. (2012) who demonstrate that in the local universe a sub-population of LERGs are hosted in blue star-forming galaxies, with these blue LERGs becoming increasingly important at higher radio powers. Thus it is possible that the contribution of such blue LERGs increases towards higher redshifts, rendering the initial assumption that all AGN are hosted by red passive galaxies invalid. Furthermore towards higher redshift we are probing towards higher luminosities, increasing the contribution of HERGs which are also preferentially hosted in galaxies with bluer colours (Best & Heckman 2012).

Figure 6. The radio luminosity function in six redshift bins to $z \sim 2.5$. The local luminosity function from Mauch & Sadler (2007) is plotted as a blue solid line. The contributions from star-forming galaxies and AGN to the local RLF are plotted as black dotted and dashed lines respectively. The green solid line represents the evolved luminosity function of the best fitting evolutionary scenario. Namely pure luminosity evolution with $\alpha_{l1}=1.90$ and $\alpha_{l2}=0.26$.

6.3   Unmatched radio sources

We considered whether excluding the 103 radio sources without reliably identified counterparts in the VIDEO survey is likely to significantly alter the RLF calculated in this paper. We achieve this by making use of redshift information available for radio sources in the Suburu/*XMM Newton* Deep field (SXDF). Simpson et al. (2012) have acquired complete redshift information (505/509 sources have redshifts) for this field by combining spectroscopic and photometric redshifts from existing deep optical and infrared photometry from Suburu (Furusawa et al. 2008) and the UKIRT Infrared Deep Sky Survey (UKIDSS; Lawrence et al. 2007) Ultra Deep Survey (UDS). As the unmatched counterparts to the VIDEO VLA survey are likely to be fainter than the adopted limits of K_s=23.8, we made the simplifying assumption that their redshift distribution could be approximated by that of the faintest, K_s>23.5, radio sources in the SXDF field. This is unlikely to be an exact match for the redshift distribution of the unmatched VIDEO sources which appear to be fainter than the limiting magnitude of the UDS survey used in Simpson et al. (2012), but is the most complete redshift information available at present.
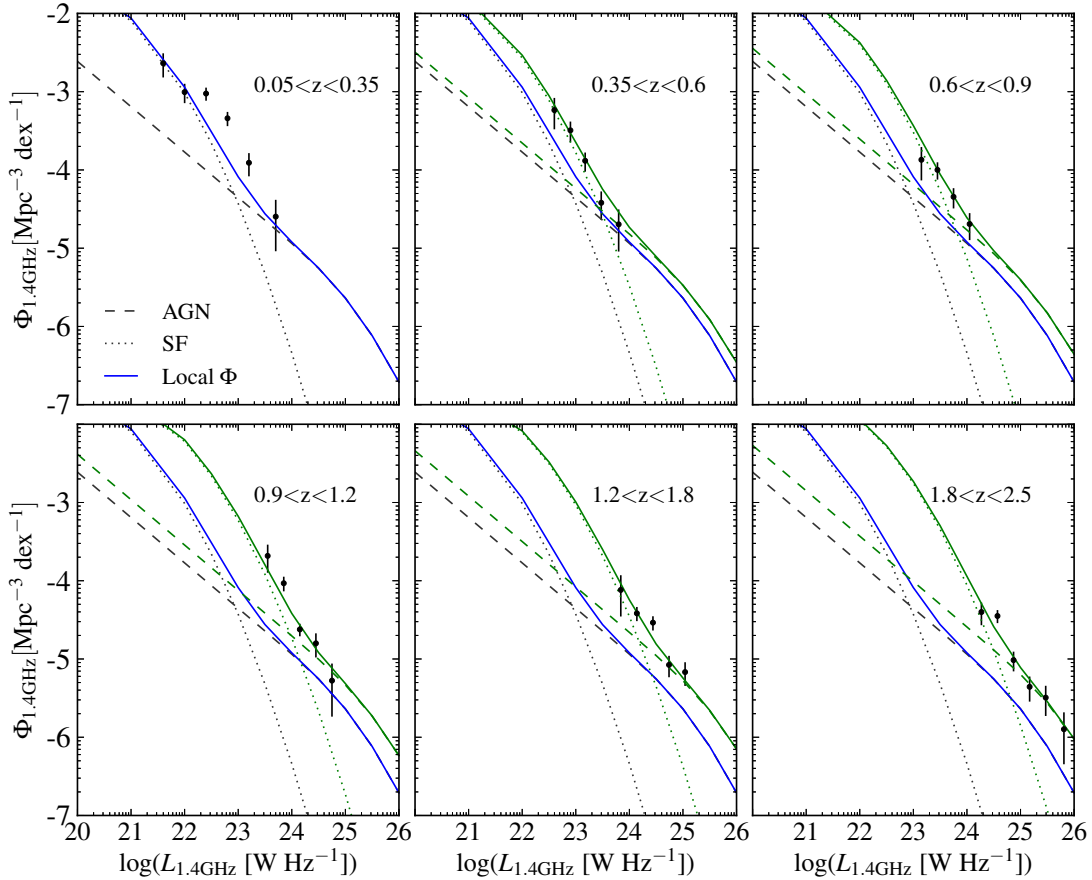
The RLF calculated by including these non-identified

radio sources via Monte Carlo simulations was found to be consistent with the RLF presented in figure 5 in all but the highest redshift bin. At the highest redshifts the luminosity function increases slightly when incorporating the unmatched sources, this slight increase is indicated by the dashed yellow line in figure 5. Thus including the unmatched sources results in stronger evolution being measured for AGN in the two component fit, and stronger evolution at z>1.2 for the combined RLF in the single component fit. The fitted values remain consistent with those reported in table 6.2 within the errors.

7   CONCLUSIONS

This paper has presented a new determination of the RLF for the VLA-VIDEO survey field using reliably identified sources with ∼10 band photometric redshifts out to z ∼2.5. The luminosity function broadly implies an increase in the space density of low luminosity ($< 10^{26}$ W Hz^{-1}) radio sources by a factor of ∼3 in the z=0–1.2 range and is consistent with slightly slower evolution out to z ∼2.5. Star forming galaxies appear to drive the stronger evolution at
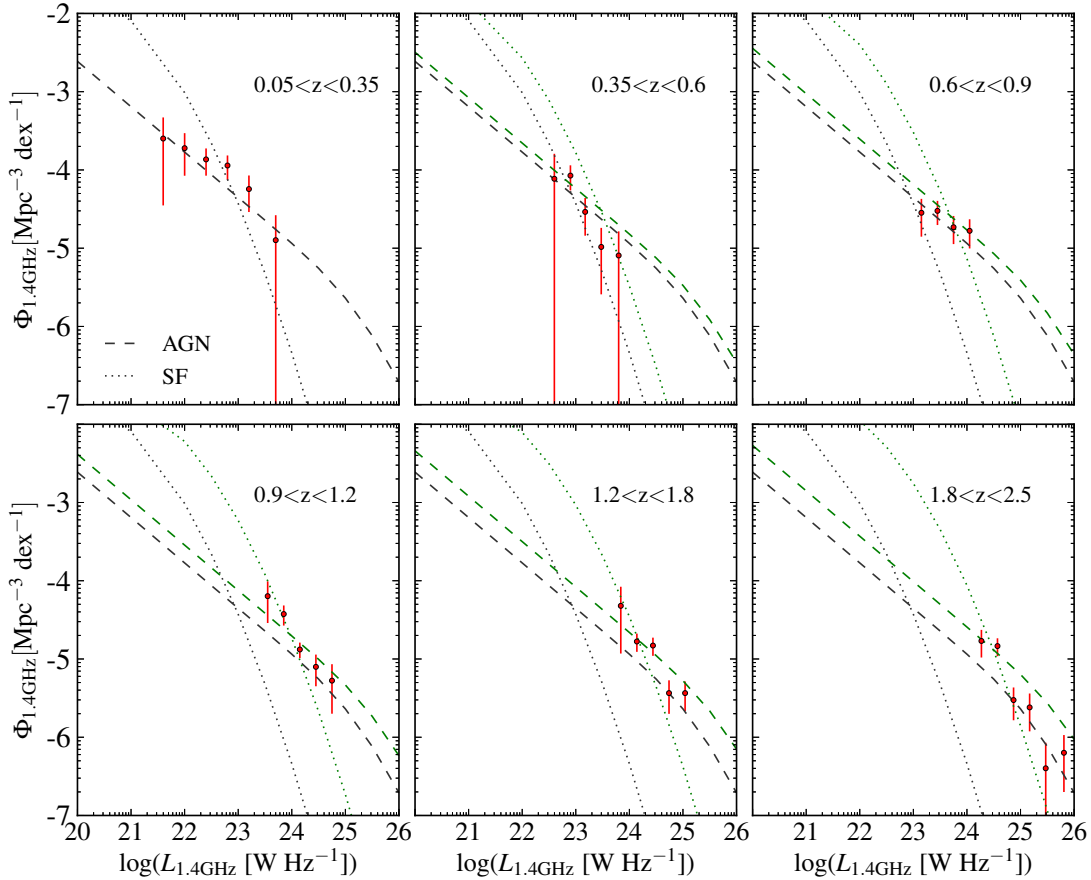
Figure 7. Radio luminosity function in six redshift bins to $z \sim 2.5$. The local luminosity function from Mauch & Sadler (2007) is plotted as a blue solid line. The contributions from star-forming galaxies and AGN to the local RLF are plotted as black dotted and dashed lines respectively. The green solid line represents the best fit to the data when allowing the AGN and star-forming RFL to evolve independently. The best fit model is pure luminosity evolution with $\alpha_l^{\mathrm{AGN}}=1.18$ and $\alpha_l^{\mathrm{SF}}=2.47$. The green dotted line is the evolved RLF of star-forming galaxies and the green dashed line is the evolved RLF of AGN.

$z<1.2$, while at higher redshifts low luminosity AGN dominate the sample, and their relatively weaker evolution results in the observed slowing down of the evolution of the RLF at $1.2<z<2.5$.

Interpreting and comparing these results to previous studies is complicated as the radio population at these lower flux densities contains contributions from radio-loud and radio-quiet AGN as well as star-forming galaxies, and these populations may all evolve independently. Previous investigations by Clewley & Jarvis (2004),Sadler et al. (2007) and Donoso et al. (2009) of large samples of bright NVSS and FIRST radio samples, with flux limits of a few mJy, imply that the low luminosity population ($<10^{25}$ W Hz^{-1}) increases by a factor of ~ 2 in the z=0–0.55 range. These studies also found evidence that the strength of the evolution taking place increases towards higher luminosities. Further support of a luminosity dependent behaviour was presented in Rigby et al. (2008) who found slightly stronger positive evolution for a smaller, fainter sample of FRI objects to redshift ~ 1. Their results imply density enhancements of ~ 5–9 for sources brighter than the 10^{25} W Hz^{-1} threshold. As this work used morphologically identified FRI candidates,

their sample is free from contamination from star-forming galaxies and these three studies should be primarily sensitive to evolution taking place in radio-loud AGN. The evolution found for AGN in the VIDEO field is slightly less than found by Sadler et al. (2007) and Rigby et al. (2008), but similar to levels detected by Donoso et al. (2009), however these works all probe the AGN evolution at low redshifts where the constraints on the AGN in our study are primarily at $0.9<z<2.5$.

There have also been several characterisations of the evolution of radio sources using very deep surveys over smaller fields, these utilise a variety of criteria to separate contributions from the different underlying populations present at fainter flux densities. Their results are thus affected by uncertainties in the completeness and contamination produced by the specific classification method employed in each case, and the use of different classification methods on a per study basis also complicates attempts to make direct comparisons between them. A summary of the results of these deeper narrower studies, which probe the luminosity function over a similar redshift range as the VIDEO study in this thesis, is presented in table 5. These works in-

Figure 8. AGN radio luminosity function in six redshift bins to $z\sim2.5$, plotted as red points. AGN are identified as objects fitted by red templates in the photometric redshift fitting procedure. The local luminosity function for star-forming galaxies and AGN (Mauch & Sadler 2007) are plotted as black dotted and dashed lines respectively. The green dotted line is the evolved RLF of star-forming galaxies and the green dashed line is the evolved RLF of AGN assuming the evolution parameters in table 6.2.

Table 5. Comparison of the current determinations of the evolution of the radio luminosity function out to a redshift of ~1.3. Numbers quoted are the α_L parameters determined by fitting pure luminosity evolution.

Reference	Field	AGN		Star-forming		All
		R-Quiet	R-Loud	Strong	Intermediate	
Strazzullo et al. (2010)	SWIRE	2.7±0.3		$3.2^{+0.4}_{-0.2}$	$3.7^{+0.3}_{-0.4}$	3.5±0.2
Smolčić et al. (2009a,b)	COSMOS	0.8±0.1		2.1±0.2		...
Padovani et al. (2011)	*Chandra* DFS	$3.8^{+0.7}_{-0.9}$	...	$3.1^{+0.8}_{-1.0}$		...
Simpson et al. (2012)	SXDF	> 0	0 [a]	...	...	> 0
This work	VIDEO	1.18±0.21		2.47±0.12		1.90± 0.17

[a] $L_{1.4GHz} \leqslant 10^{24}$ W Hz^{-1}

clude the Smolčić et al. (2009a,b) studies of the COSMOS field which use a colour based separation criteria developed from the BPT diagram to identify AGN and star-forming galaxies. Their results found pure luminosity evolution with $L^* \propto (1+z)^{0.8}$ for AGN and slightly stronger evolution in star-forming galaxies with $\alpha_L \sim 2.1$, with no separate classification for radio-quiet AGN. Their results for both AGN and star-forming galaxies thus agree reasonably well with

ours, with only slightly less evolution found for the AGN population.

In the SWIRE survey Strazzullo et al. (2010) employed a method based on SED template fitting to separate their very faint radio sample ($5\sigma \sim 14\mu$Jy) into strong and intermediate star-forming galaxies and AGN and found similar pure luminosity evolution parameters of $\alpha_L \sim 3.0$ for all three of these populations. This is higher for the AGN popula-

Figure 9. Star-forming radio luminosity function in six redshift bins to $z \sim 2.5$, plotted as blue points. Star-forming galaxies are identified as objects fitted by blue templates in the photometric redshift fitting procedure. The local luminosity function for star-forming galaxies and AGN (Mauch & Sadler 2007) are plotted as black dotted and dashed lines respectively. The green dotted line is the evolved RLF of star-forming galaxies and the green dashed line is the evolved RLF of AGN assuming the evolution parameters in table 6.2.

tion than implied by the results of Sadler et al. (2007) and Smolčić et al. (2009a) and in the work presented here. However it is consistent with previous estimates of the evolution taking place in radio-selected star-forming populations and compares well with our reported α_l of 2.47. Padovani et al. (2011) identified pure luminosity evolution at levels comparable to the SWIRE survey results taking place in both their star-forming and radio-quiet quasar samples. However they find evidence that the low luminosity radio-loud AGN population undergoes no evolution in the redshift range probed by the Smolčić et al. (2009a) study and suggested the evolution detected for low-luminosity AGN in the COSMOS study is driven by radio-quiet AGN included by their selection criteria. The evolution found for AGN sources in the VIDEO survey falls well below that found in the Padovani et al. (2011) radio-quiet population, as would be expected if the radio quiet sources form a part of the strongly evolving 'quasar' mode sources.

Simpson et al. (2012) see evidence of an increase in the number of low luminosity sources up to $z \sim 1$, their RLF increases by a factor of ~ 3 which is consistent with our work over this redshift range. As was the case in Padovani et al. (2011), they identify this enhancement as being predomi-

nantly driven by evolution of the radio-quiet objects. Radio quiet objects in their sample are identified based the ratio of mid-infrared ($24 \, \mu m$) to radio flux and this definition encompasses both star-forming and radio-quiet AGN. Whereas they see no evidence of evolution for low-luminosity radio-loud AGN.

The evolution of star-forming galaxies has also been extensively studied using optical and infrared surveys. Mid and far-infrared *Spitzer* observations imply a galaxy population undergoing pure luminosity evolution with $\alpha_l \sim 3.4$–3.8 out to $z \sim 1.2$ (e.g. Caputi et al. 2007; Magnelli et al. 2009; Rujopakarn et al. 2010; Magnelli et al. 2011). While far-infrared luminosity functions from *Herschel* data result in slightly stronger evolution estimates with $L_* \propto (1+z)^{4.1 \pm 0.3}$ up to $z \sim 1.5$ (Gruppioni et al. 2010; Lapi et al. 2011). At lower redshifts ($z < 0.5$) some *Herschel* studies have seen evidence of stronger evolution in star-forming galaxies with the total luminosity density evolving as $(1+z)^{7.1}$ (Dye et al. 2010). These recent infrared studies are broadly consistent with the radio derived star-formation histories in table 5 implying a very similar increase in the total cosmic star formation density in the interval between $z \sim 0$–1. The radio results are also in good agreement (e.g. Smolčić et al.

2009b, figure 6) with earlier works using UV-derived star-formation estimates (Wolf et al. 2003; Arnouts et al. 2005; Baldry et al. 2005, see also Hopkins & Beacom 2006).

Beyond $z \sim 1.2$ there have been some suggestions of a cutoff in the RLF (Waddington et al. 2001; Rigby et al. 2008, 2011). The LF of Simpson et al. (2012) also implies systematically lower space densities for low radio luminosity objects at redshifts >1.5 whilst Padovani et al. (2011) claim evidence of strong negative evolution in the more powerful radio-loud populations which they suggest might be the result of a high redshift cutoff in these source populations. However figure 5 indicates that the RLF continues to increase out to $z \sim 2.5$, although the rate of increase does slow beyond $z \sim 1.2$. Disentangling the contributions of the various low-luminosity radio populations is clearly a difficult proposition and has important implications for our ability to deduce their evolutionary behaviour and make inferences about links between AGN and star- forming processes. The discussion above which presents the myriad of evolutionary scenarios currently postulated serves to illustrate how much uncertainty remains in this area and the vitally important role of multi-wavelength datasets in constraining these increasingly complex evolutionary scenarios.

More complicated modelling of the evolution of radio sources could be carried out by combining a range of deep fields, e.g. COSMOS (Smolčić et al. 2009a,b), SXDF (Simpson et al. 2012) and the VLA-VIDEO field in this work and combining surveys with different flux limits provides much better coverage of the luminosity-redshift plane (see e.g. Rigby et al. 2011). Future deeper surveys with SKA pathfinder telescopes, such as MeerKAT will allow us to explore the the evolution of radio sources over larger areas and to much higher redshifts ($z \sim 4$) overcoming the sample variance limitations of current small area surveys.

REFERENCES

Adami C., et al., 2011, A&A, 526, A18
Allen S. W., Dunn R. J. H., Fabian A. C., Taylor G. B., Reynolds C. S., 2006, MNRAS, 372, 21
Arnouts S., et al., 2005, ApJ, 619, L43
Babbedge T. S. R., et al., 2004, MNRAS, 353, 654
Baldi R. D., Capetti A., 2008, A&A, 489, 989
Baldry I. K., et al., 2005, MNRAS, 358, 441
Ball N. M., Brunner R. J., Myers A. D., Strand N. E., Alberts S. L., Tcheng D., 2008, ApJ, 683, 12
Bertin E., Arnouts S., 1996, A&A Supplement, 117, 393
Best P. N., Heckman T. M., 2012, MNRAS, 421, 1569
Best P. N., Kaiser C. R., Heckman T. M., Kauffmann G., 2006, MNRAS, 368, L67
Bîrzan L., Rafferty D. A., McNamara B. R., Wise M. W., Nulsen P. E. J., 2004, ApJ, 607, 800
Bondi M., et al., 2003, A&A, 403, 857
Bondi M., et al., 2007, A&A, 463, 519
Bower R. G., Benson A. J., Malbon R., Helly J. C., Frenk C. S., Baugh C. M., Cole S., Lacey C. G., 2006, MNRAS, 370, 645
Caputi K. I., Lagache G., Yan L., Dole H., Bavouzet N., Le Floc'h E., Choi P. I., Helou G., Reddy N., 2007, ApJ, 660, 97
Cardamone C. N., et al., 2010, ApJS, 189, 270
Cattaneo A., et al., 2009, Nature, 460, 213
Ciliegi P., et al., 2003, A&A, 398, 901
Clewley L., Jarvis M. J., 2004, MNRAS, 352, 909
Croton D. J., et al., 2006, MNRAS, 365, 11
de Ruiter H. R., Arp H. C., Willis A. G., 1977, A&AS, 28, 211
Di Matteo T., Springel V., Hernquist L., 2005, Nature, 433, 604
Donoso E., Best P. N., Kauffmann G., 2009, MNRAS, 392, 617
Dunlop J. S., Peacock J. A., 1990, MNRAS, 247, 19
Dye S., et al., 2010, A&A, 518, L10
Evans D. A., Worrall D. M., Hardcastle M. J., Kraft R. P., Birkinshaw M., 2006, ApJ, 642, 96
Ferrarese L., Merritt D., 2000, ApJ, 539, L9
Furusawa H., et al., 2008, ApJS, 176, 1
Gebhardt K., et al., 2000, ApJ, 539, L13
Gruppioni C., et al., 2010, A&A, 518, L27
Hardcastle M. J., Ching J. H. Y., Virdee J. S., Jarvis M. J., Croom S. M., et al., 2013, MNRAS, 429, 2407
Hardcastle M. J., Evans D. A., Croston J. H., 2006, MNRAS, 370, 1893
Hardcastle M. J., Evans D. A., Croston J. H., 2007, MNRAS, 376, 1849
Hardcastle M. J., Evans D. A., Croston J. H., 2009, MNRAS, 396, 1929
Herbert P. D., Jarvis M. J., Willott C. J., McLure R. J., Mitchell E., Rawlings S., Hill G. J., Dunlop J. S., 2010, MNRAS, 406, 1841
Herbert P. D., Jarvis M. J., Willott C. J., McLure R. J., Mitchell E., Rawlings S., Hill G. J., Dunlop J. S., 2011, MNRAS, 410, 1360
Heywood I., Jarvis M. J., Condon J., 2013, arXiv:1302.2010
Hopkins A. M., Beacom J. F., 2006, ApJ, 651, 142
Huynh M. T., Jackson C. A., Norris R. P., Fernandez-Soto A., 2008, AJ, 135, 2470

Ilbert O., et al., 2006, A&A, 457, 841

Ilbert O., et al., 2009, ApJ, 690, 1236

Janssen R. M. J., Röttgering H. J. A., Best P. N., Brinchmann J., 2012, A&A, 541, A62

Jarvis M., Rawlings S., 2004, New Astronomy Reviews, 48, 1173

Jarvis M. J., et al., 2013, MNRAS, 428, 1281

Jarvis M. J., Rawlings S., 2000, MNRAS, 319, 121

Jarvis M. J., Rawlings S., Willott C. J., Blundell K. M., Eales S., Lacy M., 2001, MNRAS, 327, 907

Jones D. H., et al., 2004, MNRAS, 355, 747

Kellermann K. I., Sramek R., Schmidt M., Shaffer D. B., Green R., 1989, AJ, 98, 1195

Kormendy J., Richstone D., 1995, ARA&A, 33, 581

Laing R. A., Riley J. M., Longair M. S., 1983, MNRAS, 204, 151

Lapi A., et al., 2011, ApJ, 742, 24

Lawrence A., et al., 2007, MNRAS, 379, 1599

Le Fèvre O., Vettolani G., Garilli B., Tresse L., Bottini D., Le Brun V., Maccagni D., et al., 2005, A&A, 439, 845

Longair M. S., 1966, MNRAS, 133, 421

Magnelli B., Elbaz D., Chary R. R., Dickinson M., Le Borgne D., Frayer D. T., Willmer C. N. A., 2009, A&A, 496, 57

Magnelli B., Elbaz D., Chary R. R., Dickinson M., Le Borgne D., Frayer D. T., Willmer C. N. A., 2011, A&A, 528, A35

Magorrian J., et al., 1998, AJ, 115, 2285

Mauch T., Sadler E. M., 2007, MNRAS, 375, 931

McAlpine K., Jarvis M. J., 2011, MNRAS, 413, 1054

McAlpine K., Smith D. J. B., Jarvis M. J., Bonfield D. G., Fleuren S., 2012, MNRAS, 423, 132

McLure R. J., Dunlop J. S., 2002, MNRAS, 331, 795

McNamara B. R., Wise M., Nulsen P. E. J., David L. P., Sarazin C. L., Bautz M., Markevitch M., Vikhlinin A., Forman W. R., Jones C., Harris D. E., 2000, ApJ, 534, L135

Merloni A., Heinz S., 2007, MNRAS, 381, 589

Merloni A., Rudnick G., Di Matteo T., 2007, in Aschenbach B., Burwitz V., Hasinger G., Leibundgut B., eds, ESO Astrophysics Symposia Relativistic Astrophysics Legacy and Cosmology - Einstein's Legacy, Springer-Verlag, Berlin, p. 158

Mobasher B., et al., 2004, ApJ Letters, 600, L167

Novikov I. D., Thorne K. S., 1973, in Dewitt C., Dewitt B. S., eds, Black Holes (Les Astres Occlus), Gordon and Breach, New York, p. 343

Ogle P., Whysong D., Antonucci R., 2006, ApJ, 647, 161

Pacaud F., et al., 2007, MNRAS, 382, 1289

Padovani P., Mainieri V., Tozzi P., Kellermann K. I., Fomalont E. B., Miller N., Rosati P., Shaver P., 2009, ApJ, 694, 235

Padovani P., Miller N., Kellermann K. I., Mainieri V., Rosati P., Tozzi P., 2011, ApJ, 740, 20

Polletta M., et al., 2007, ApJ, 663, 81

Richards G. T., et al., 2001, AJ, 122, 1151

Rigby E. E., Best P. N., Brookes M. H., Peacock J. A., Dunlop J. S., Röttgering H. J. A., Wall J. V., Ker L., 2011, MNRAS, 416, 1900

Rigby E. E., Best P. N., Snellen I. A. G., 2008, MNRAS, 385, 310

Rujopakarn W., Eisenstein D. J., Rieke G. H., Papovich C., Cool R. J., Moustakas J., Jannuzi B. T., Kochanek C. S., Rieke M. J., Dey A., Eisenhardt P., Murray S. S., Brown M. J. I., Le Floc'h E., 2010, ApJ, 718, 1171

Sadler E. M., et al., 2007, MNRAS, 381, 211

Salvato M., et al., 2009, ApJ, 690, 1250

Salvato M., et al., 2011, ApJ, 742, 61

Schmidt M., 1968, ApJ, 151, 393

Seymour N., et al., 2007, ApJ Supplement Series, 171, 353

Shakura N. I., Sunyaev R. A., 1973, A&A, 24, 337

Silk J., Rees M. J., 1998, A&A, 331, L1

Simpson C., et al., 2006, MNRAS, 373, L21

Simpson C., et al., 2012, MNRAS, 421, 3060

Smolčić V., et al., 2008, ApJ Supplement Series, 177, 14

Smolčić V., et al., 2009a, ApJ, 696, 24

Smolčić V., et al., 2009b, ApJ, 690, 610

Smolčić V., Riechers D. A., 2011, ApJ, 730, 64

Strazzullo V., Pannella M., Owen F. N., Bender R., Morrison G. E., Wang W.-H., Shupe D. L., 2010, ApJ, 714, 1305

Sutherland W., Saunders W., 1992, MNRAS, 259, 413

Tremaine S., et al., 2002, ApJ, 574, 740

Urry C. M., Padovani P., 1995, PASP, 107, 803

Waddington I., Dunlop J. S., Peacock J. A., Windhorst R. A., 2001, MNRAS, 328, 882

Wall J. V., Jackson C. A., Shaver P. A., Hook I. M., Kellermann K. I., 2005, A&A, 434, 133

Willott C. J., Rawlings S., Blundell K. M., Lacy M., Eales S. A., 2001, MNRAS, 322, 536

Wilman R. J., et al., 2008, MNRAS, 388, 1335

Wilman R. J., Jarvis M. J., Mauch T., Rawlings S., Hickey S., 2010, MNRAS, 405, 447

Wolf C., et al., 2004, A&A, 421, 913

Wolf C., Meisenheimer K., Rix H.-W., Borch A., Dye S., Kleinheinrich M., 2003, A&A, 401, 73